Geophysical Journal International

Geophys. J. Int. (2020) **222,** 1270–1282 doi: 10.1093/gji/ggaa254

GJI Seismology

Geometric controls on megathrust earthquakes

Steven M. Plescia [1,2] and Gavin P. Hayes[1]

[1] *U.S. Geological Survey, National Earthquake Information Center, Golden, CO, USA. E-mail: steven.plescia@colorado.edu*

[2] *Department of Geological Sciences and Cooperative Institute for Research in Environmental Sciences (CIRES), University of Colorado, Boulder, CO, USA*

Accepted 2020 May 8. Received 2020 May 7; in original form 2019 August 6

SUMMARY

The role of subduction zone geometry in the nucleation and propagation of great-sized earthquake ruptures is an important topic for earthquake hazard, since knowing how big an earthquake can be on a given fault is fundamentally important. Past studies have shown subducting bathymetric features (e.g. ridges, fracture zones, seamount chains) may arrest a propagating rupture. Other studies have correlated the occurrence of great-sized earthquakes with flat megathrusts and homogenous stresses over large distances. It remains unclear, however, how subduction zone geometry and the potential for great-sized earthquakes (M 8+) are quantifiably linked—or indeed whether they can be. Here, we examine the potential role of subduction zone geometry in limiting earthquake rupture by mapping the planarity of seismogenic zones in the Slab2 subduction zone geometry database. We build from the observation that historical great-sized earthquakes have preferentially occurred where the surrounding megathrust is broadly planar, and we use this relationship to search for geometrically similar features elsewhere in subduction zones worldwide. Assuming geometry exerts a primary control on earthquake propagation and termination, we estimate the potential size distribution of large (M 7+) earthquakes and the maximum earthquake magnitude along global subduction faults based on geometrical features alone. Our results suggest that most subduction zones are capable of hosting great-sized earthquakes over much of their area. Many bathymetric features previously identified as barriers are indistinguishable from the surrounding megathrust from the perspective of slab curvature, meaning that they either do not play an important role in arresting earthquake rupture or that their influence on slab geometry at depth is not resolvable at the spatial scale of our subduction zone geometry models.

Key words: Earthquake hazards; Earthquake source observations; Seismicity and tectonics; Subduction zone processes.

INTRODUCTION

The seismic hazard associated with great-sized earthquakes ($M_w > 8$) that occur in subduction zones makes understanding why they rupture, and where they can rupture, important questions. Seismicity across subduction zones varies greatly even at length scales of tens of kilometres. Where great-sized earthquake ruptures occur and why these ruptures occur in those locations have led seismologists to look for a correlation between maximum magnitude for a given region and a broad variety of geological and geometrical parameters.

For example, Uyeda & Kanamori (1979) and Ruff & Kanamori (1980) proposed that a young, light plate subducting at a high rate produces a compressive stress field and large earthquakes, and an old heavy slab subducting slowly leads to an extensional stress field and smaller earthquakes. However, the recent M 9.1 2004 Sumatra and M 9.1 2011 Tohoku-Oki earthquakes challenge this model. Nishikawa & Ide (2014) correlated b-value with subducting plate age and plate motion, because b-value is considered to be a proxy for shear stress and decreases relative to interseismic values before a great-sized earthquake. They found that a younger plate correlates with low b-values, but they found no correlation between plate motion and b-values. Because younger plates tend to be warm and more buoyant, they suggested that buoyancy may be the primary control on the earthquake size distribution in subduction zones. Others have proposed that negative gravity anomalies along the trench correlate with the rupture zones of large earthquakes, implying that forearc structure may be a major control (e.g. Song & Simons 2003; Bassett *et al.* 2016). Sediment thickness (trench fill $\geq$1 km) has also been found to have a statistically significant correlation with giant earthquake occurrence (e.g. Heuret *et al.* 2012), as has seafloor roughness (e.g. van Rijsingen *et al.* 2018). Recently, the curvature of the slab in the along-dip (Ks) and the along-strike (Kt) directions has also been shown to have a significant correlation with the maximum magnitude of historical events in a seismogenic zone (Bletery

et al. 2016). Because this planarity model is shown to correlate more strongly with historical maximum magnitude than many other parameters (Bletery *et al.* 2016), and because we can directly test the hypothesis with a new generation of slab geometry models (Hayes *et al.* 2018), we choose here to investigate this further.

In this paper, we examine the slab curvature of subduction zone models in the newly published Slab2 subduction zone geometry database (Hayes *et al.* 2018) and use it to examine the geometric controls on megathrust earthquakes. We look for areas along a subduction zone that are geometrically similar to historical M 8 + earthquakes (here, historical is used with specific reference to post-1900 events) and use scaling relations (e.g. Allen & Hayes 2017) to determine the potential for these areas to host large magnitude earthquakes in the future.

METHOD

Bletery *et al.* (2016) show that very large (M 8.5+) earthquakes preferentially rupture planar, or flat (low-curvature) megathrust interfaces; they do this highlighting a spatial correlation between the rupture areas of such earthquakes, with the gradient of subduction zone dip ('flatness', or 'planarity') calculated from the Slab1.0 subduction zone geometry database (Hayes *et al.* 2012). If we assume that this correlation is representative of long-term behaviour, then it is also reasonable to assume that the geometric characteristics of the megathrust within the rupture zones of very large historical earthquakes can be used as a signature for where such earthquakes can occur—and, thus, if one maps out the geometric characteristics of all megathrusts, identifying regions with similar characteristics allows us to quantitatively map where very large earthquakes might occur in the future. This is the essence of what we attempt here. We analyse along-dip curvature, Ks (Ks $= \mathrm{d}\theta/\mathrm{d}s$, where θ is the dip angle and s is the tangent to the interface in the downdip direction, following Bletery *et al.* 2016), along-strike curvature, Kt (Kt $= \mathrm{d}\theta/\mathrm{d}t$, where t is the tangent to the interface in the along-strike direction), and the combination of the two. The majority of our discussions below focus on results from using the combination of the two parameters; Figs S1–S6 present Ks and Kt separately for all subduction zones. Our workflow is explained in detail below and can be summarized as follows:

(1) Calculate Ks and Kt for each subduction zone.

(2) Within the rupture areas of historical earthquakes, calculate the mean values of Ks and Kt, and their respective standard deviations. These mean values become what we refer to as 'target curvature', since we wish to identity where else these geometrical features exist.

(3) Next we search for where these target values exist over a large enough contiguous area to host a large- to great-sized earthquake, by creating polygons whose mean planarity must average to less than the target curvature plus standard deviation (i.e. Ks $\leq \mathrm{Ks_{tar}} + \sigma_{\mathrm{Ks}}$; Kt $\leq \mathrm{Kt_{tar}} + \sigma_{\mathrm{Kt}}$). Polygons increase in size until adding extra sides increases their average planarity above the target values (plus standard deviation).

(4) We use these polygons to examine the size distribution of geometrically controlled large (M 7+) earthquakes in each subduction zone.

(5) Finally, we combine overlapping polygons to create a maximum rupture area and use this to calculate the maximum magnitude of a geometrically controlled rupture (M_{flat}).

Prior to beginning our analysis, we first verified that the correlation between maximum magnitude, Ks and Kt were not dependent on the Slab1.0 model itself (see Fig. S7), the geometry model used in Bletery *et al.* (2016). We then replaced the Slab1.0 subduction zone geometry database with Slab2. Slab2 (Hayes *et al.* 2018) improves upon Slab1.0 by incorporating significantly more data that image subducting slabs (e.g. significantly expanded active source data, relocated regional seismicity catalogues, seismic tomography, receiver functions) and by using an improved methodology that directly solves for subduction zone geometry in three dimensions, rather than the 2-D-to-3-D step used in Slab1.0. Slab2 also contains almost double the number of subduction zones than are included in Slab1.0, and in particular provides models for less active and/or more complex subduction zones, allowing us to conduct a more comprehensive study representative of the complete range of subduction zone activity. Further details of the differences between these models are given in the Supporting Information.

In order to determine a target curvature ($\mathrm{Ks_{tar}}$, $\mathrm{Kt_{tar}}$) value for our searches, we calculated Ks and Kt for all subduction zones in Slab2 with well-constrained seismogenic zone limits (seismogenic zone depth limits are taken from Table 1 of Hayes *et al.* (2018); see Supplementary Text *'Selection of Subduction Zones'* for discussion of this procedure, and of slabs excluded from our analysis because of a lack of data) and correlated this with the rupture areas of historical M 8.0–M 8.9 20th and 21st century earthquakes that occurred within the seismogenic zone of their respective megathrusts (22 events across eight different subduction zones). We excluded data from within rupture zones of M 8.9 + earthquakes because the geometric characteristics of those regions are different from (i.e. more planar than), and much larger than, those regions hosting smaller (but still great-sized) earthquakes. We did this to avoid biasing our analysis towards overly planar slab segments. We also note that our seismogenic zone limits are defined using the distribution of hypocentres of historical moderate-to-large thrust-faulting earthquakes within each region. Therefore, our seismogenic zone limits may not reflect the entire seismogenic zone width capable of slipping in great-sized earthquake ruptures, given that the latter have been known to propagate into regions at the up- and downdip ends of seismogenic zones that are traditionally thought to be stable or conditionally stable (Lay *et al.* 2012).

For both Ks and Kt, we calculated the mean ($\mathrm{Ks_{tar}}$; $\mathrm{Kt_{tar}}$) and standard deviation (σ_{Ks}; σ_{Ks}) within each historical rupture zone; all events were then averaged to compute a mean and standard deviation representative of M 8 events globally (Fig. 1; green lines). For the eight subduction zones with historical M 8.0–M 8.9 ruptures, a regional average value was also calculated (Fig. 1; blue diamonds). We focus our discussion on the globally averaged values as they are less sensitive to outliers and allow us to search all global subduction zones regardless of whether or not they have hosted a historical M 8 + earthquake. We have also carried out a series of sensitivity tests to establish how our results are influenced by the absolute value of this global threshold (see Fig. S8), indicating that at least in South America, adjusting $\mathrm{Ks_{tar}}$ to lower values leads to fewer historical ruptures being identified as sufficiently planar for future large events.

Next, we perform a systematic grid search through Slab2 models to determine where else these geometric characteristics exist. Our grid search creates rectangular polygons by choosing a point that is below the defined threshold values (Ks $\leq \mathrm{Ks_{tar}} + \sigma_{\mathrm{Ks}}$, and Kt $\leq \mathrm{Kt_{tar}} + \sigma_{\mathrm{Kt}}$; that is more planar than the target value) and then attempts to add a point in the along-strike direction. If the geometric characteristics of the pair of points is still below the threshold, the

Table 1. Area and magnitude distributions of geometrically controlled fault patches for each subduction zone (columns 2–6), and equivalent M_{flat} calculations for combined polygons in each region. *N* describes the number of individual polygons passing magnitude and aspect ratio filters; mean A and SD_A describe the average area of these polygons, and their standard deviation. Equivalent magnitude and range (mean ± one standard deviation) are also listed. For M_{flat}, *M* 9.5 + means the combined polygon area exceeds the upper limit of most scaling relations. A M_{flat} < 8 means our search did not identify any polygons large enough to host a *M*8. Our analysis did not identify any polygons large enough to host *M*7 + earthquakes in Manila. See Table S1 for a complete list of historical *M*8 + post-1900 earthquakes, from which historical M_{max} values are taken (see also Advanced National Seismic System Comprehensive Catalogue, http://earthquake.usgs.gov/earthquakes/search/).

Region	*N*	Mean A (m^2)	SD_A (m^2)	Mean M_w	M_w range	M_{flat}	Historical M_{max}
Alaska-Aleutians (alu)	346	7.62E + 09	1.01E + 10	7.8	7.4–8.1	9.5+	9.2
Central America (cam)	69	5.04E + 09	4.22E + 09	7.7	6.9–7.9	8.8	8.1
Caribbean (car)	160	1.21E + 10	1.35E + 10	8.0	7.2–8.2	9.3	8.4*
Cascadia (cas)	63	3.07E + 10	2.41E + 10	8.3	7.6–8.6	9.2	9.0*
Izu-Bonin (izu)	264	6.21E + 09	5.07E + 09	7.7	7.1–7.9	9.2	7.5
Kermadec (ker)	279	9.16E + 09	1.33E + 10	7.9	7.6–8.3	9.5+	8.3
Kamchatka-Kuril-Japan (kur)	368	1.13E + 10	1.67E + 10	7.9	7.7–8.3	9.5+	9.1
Makran (mak)	103	2.06E + 10	1.72E + 10	8.1	7.5–8.4	9.3	8.1
Philippines (phi)	3	6.51E + 09	3.04E + 09	7.7	7.5–7.9	8.0	7.8
New Guinea (png)	83	1.06E + 10	1.68E + 10	8.0	7.8–8.4	9.2	8.2
Ryukyu (ryu)	132	5.80E + 09	5.74E + 09	7.7	5.7–8.0	9.2	8.8
South America (sam)	674	1.09E + 10	1.32E + 10	7.9	7.4–8.2	9.5+	9.5
Scotia (sco)	26	4.53E + 09	1.77E + 09	7.6	7.4–7.7	8.0	7.5
Solomon Islands (sol)	20	1.83E + 09	1.01E + 09	7.2	6.9–7.4	8.1	8.1
Sulawesi (sul)	32	2.31E + 09	1.09E + 09	7.3	7.1–7.5	8.2	7.9
Sumatra (sum)	524	1.30E + 10	1.61E + 10	8.0	7.5–8.3	9.5+	9.1
Vanuatu (van)	5	1.33E + 09	1.42E + 08	7.1	7.0–7.1	7.2	8.0

*** Pre-20th century; see Hough (2013) and Satake *et al.* (1996).

point is added to our search polygon. The search alternates between adding points in an along-strike and along-dip direction eventually evolving to adding entire sides rather than singular points once the search polygon is large enough. The search continues until it cannot add another point/side, in any direction, without increasing the polygon Ks and Kt above Ks_{tar} and Ks_{tar}, respectively.

Once the search has stopped, we compare the size of the polygon to scaling relations for subduction zone earthquakes (Mai & Beroza 2000; Leonard 2010; Muratoni *et al.* 2013; Goda *et al.* 2016; Skarlatoudis *et al.* 2016; Ye *et al.* 2016; Allen & Hayes 2017). We use seven different scaling relations to compute equivalent magnitude for each polygon area, retaining the median value for each. We remove polygons with an aspect ratio (length/width) less than 0.5, and greater than 10, as all known historical events lie within this range (the 2004 Sumatra rupture, the longest known historical rupture, had an aspect ratio of approximately 8.5). Any grid points that lie within a retained search polygon are no longer considered as a potential starting point for subsequent polygons in our grid search. In this way, we identify areas of subduction zones with broadly planar features characteristic of large earthquake ruptures. This allows us to map a distribution of planar fault patches for each subduction zone, such that we can construct a spatial distribution of where large and great-sized earthquakes might be likely based on planarity alone (Fig. 2), and also how many such fault patches exist for a given subduction zone (Fig. 3).

Next, once every point within the seismogenic zone of a given Slab2 model has been analysed, overlapping search polygons are stitched together (Figs 4–6). The area of these combined polygons is then used to approximate the potential largest magnitude earthquake that could occur in that region, from a purely geometric perspective (Table 1). We call this magnitude M_{flat}. To calculate M_{flat}, we use the same scaling relations listed above, taking the median of resulting magnitudes as our preferred M_{flat} estimate. We recognize that this step in particular is fraught with uncertainty, not least because these scaling relations were designed predominantly based on earthquakes smaller than the largest equivalent areas encountered here, and extrapolating beyond the bounds of their data input is dangerous. Nevertheless, the analysis provides a means by which we can compare one subduction zone to another in a relative sense. It also allows us to evaluate whether geometric characteristics exist that might consistently arrest rupture. Thus, while the absolute M_{flat} values involve uncertainty, a comparison of their relative size is informative.

RESULTS

Figs 2 and 3 show the equivalent approximate magnitude distributions of geometrically controlled fault patches for each subduction zone. If we assume that rupture is limited to only one such fault patch in a given earthquake, then these can be interpreted to indicate where great-sized and mega-earthquake ruptures are more or less likely. For example, the seismogenic zones adjacent to southern Chile, Ecuador, Cascadia, Alaska, Japan and Sumatra are all broadly planar enough for *M*∼9 sized earthquakes—indeed, each of these regions has hosted one or more events of this approximate size in the past. Conversely, however, similar sized events appear possible adjacent to the southern Lesser Antilles, northern Kermadec, New Guinea and Makran subduction zones, none of which have hosted earthquakes much larger than *M*∼8 historically. Further, the subduction zone adjacent to Kamchatka, which hosted a *M*∼9 earthquake in 1952, is not highlighted in this analysis. We interpret this to indicate that our analysis is indicative only of where subduction zones have the geometric characteristics capable of supporting large earthquake rupture and that other factors—principally fault coupling—must also be considered to evaluate the likelihood of such events. In regions such as Kamchatka, where no single patch appears large enough to support *M* 9 + events, our analysis may indicate that for such events to occur, multiple fault patches must combine into larger ruptures. We expand upon this issue below.

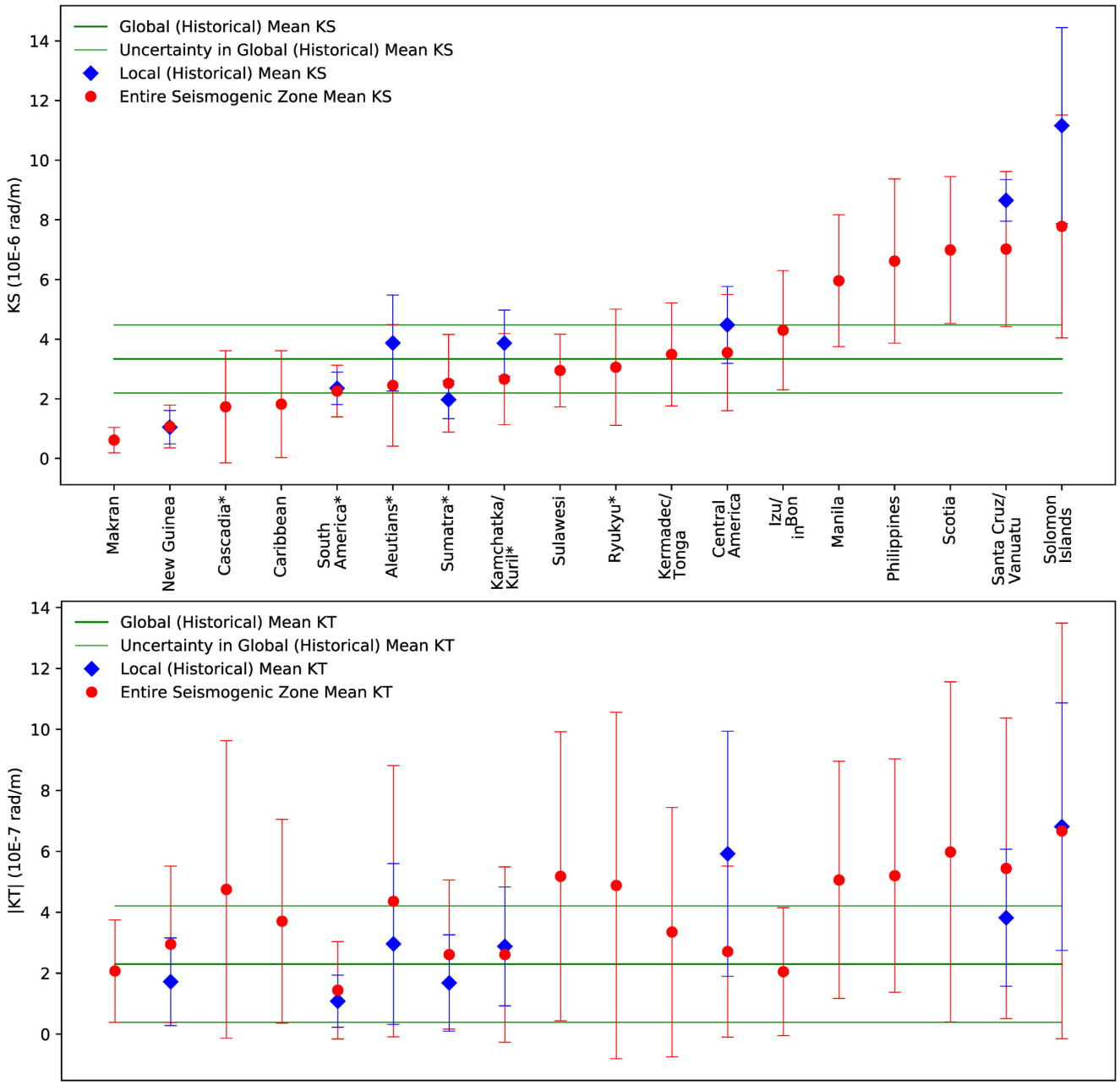

Figure 1. The mean along-dip slab planarity (Ks, top panel) and along-strike planarity (Kt, bottom panel) for each seismogenic zone, ordered from left-right by increasing Ks. The mean of each seismogenic zone (red) can be compared to the regional historical M 8.0–8.9 events (blue) or global (green) threshold to determine how likely the region is to host future large earthquakes. If planarity for a given subduction zone (including uncertainties) is far below the green line, then most of the seismogenic zone is likely to be identified as having potential for future rupture in our search. Conversely, if planarity lies well above the green line, then fewer polygons will be identified during our search. Subduction zones marked with a star have hosted a historical M 8.5 + earthquake.

Magnitude distributions in Fig. 3 may provide hints regarding the potential relative rates of large versus great-sized earthquakes in each subduction zone—again, under the assumption of geometrically controlled single-patch rupture. Observing differences between subduction zones is particularly interesting—several appear to demonstrate Gutenberg–Richter like distributions (e.g. South America, Sumatra and Alaska), while others appear to suggest much more characteristic behaviour (e.g. Cascadia, Makran), or a mix of the two (e.g. New Guinea). Caution is necessary in interpreting these distributions, however, since—as previously noted—there is not a one-to-one correlation between where large earthquakes can occur according to this analysis and where they have been observed historically.

As previously discussed, discrepancies between historical earthquake size and single fault-patch size in our analysis for a given subduction zone may imply the necessity for, or existence of, multiple-patch ruptures in those regions. In Figs 4–6, we show combined polygons for all subduction zones. These illustrate that while individual polygons may be limited in their spatial extent, in many places those polygons overlap considerably, and thus their combination implies that several subduction zones are broad and planar over much of their area.

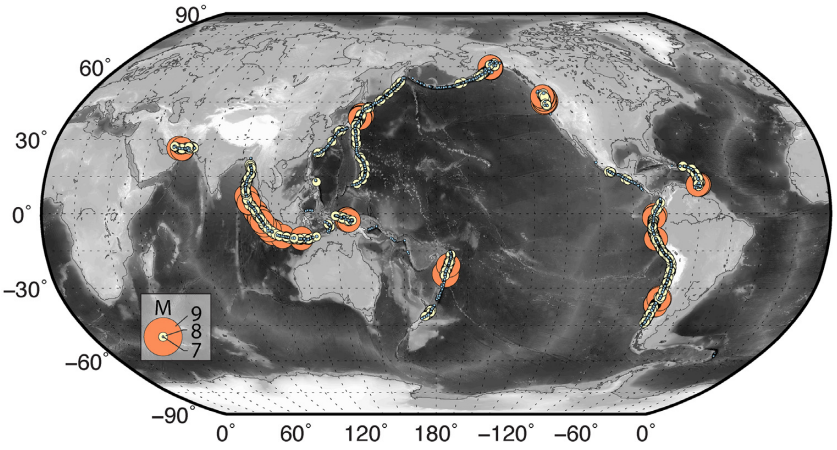

Figure 2. The global distribution of large individual polygons identified in our joint Ks-Kt planarity search, sized according to their equivalent magnitude from scaling relations. See main text and Table 1 for details.

In the Alaska-Aleutians subduction zone (Fig. 4a), polygons capable of hosting large- to great-sized earthquakes are identified over almost the whole length of the arc. A short gap exists just to the west of Bowers Ridge at about 175°E. Historically, M 8 + earthquakes have occurred along most of the arc, the largest being the M 9.2 1964–03-28 event beneath Alaska. The gap in combined polygons lies within the 1965 M 8.7 Rat Island rupture zone. Our models do not identify the Shumagin Gap, an area which has not seen a great-sized earthquake since possibly 1903 (Davies *et al.* 1981), as being geometrically distinct from the surrounding region.

In Central America (Fig. 4b), we modified the seismogenic zone width such that it is limited to depths shallower than the flat portion of the slab in Mexico, based on evidence from slow slip and tremor analyses (e.g. Graham *et al.* 2016). Nevertheless, polygons capable of hosting large- to great-sized earthquakes are still identified over much of the length of the arc. Additionally, there areas overlap such that the combined polygon extends from northern Mexico to the Honduras-Nicaragua border. This area encapsulates the 1985 Michoacan rupture, but the 1995 Colima earthquake rupture lies farther northwest within an area of higher curvature (Fig. 4b). The largest documented historical event occurred along the coast from Guerrero, Mexico, to Tehuantepec in Oaxaca, Mexico, in 1787 with M ∼8.6 (Suarez & Albini 2009) and encompassed many of the rupture zones of the more recent smaller events (Bilek & Lay 2018). Because of the shallower downdip limit of the seismogenic zone in this region, we find M_{flat} ∼8.8. This magnitude is slightly larger than the historical maximum (though such an earthquake would likely rupture a much greater area). Our models do not identify the Tehuantepec Ridge as a significant barrier to rupture.

In the Sunda subduction zone (Fig. 4c), no clear break in the planarity is apparent over most of the seismogenic zone extending all the way from the Andaman Islands in the northwest to Timor Island in the southeast. In East Timor and farther east, curvature appears high enough to prevent through-going rupture. Historically, great-sized earthquakes have occurred west of 105°E, offshore Sumatra. We find no geometric reason in any of our models why a M 8 + event has not occurred in the past century east of 110°E, south of Java.

In the Vanuatu subduction zone (Fig. 4d), curvature is both high and highly variable, such that very few areas appear planar enough to host great-sized earthquakes based on our analysis. M 8 + ruptures have occurred at the northernmost extent of the subduction zone in 2013 (M 8.0), and adjacent to the southern Vanuatu islands in 1920 (M 8.1). Planar slab geometry is observed in both of these regions; though in both cases, these areas occur at the downdip end of the seismogenic zone and do not extend to the trench. In contrast, at least the 2013 event is thought to have ruptured close to the trench, resulting in a large local tsunami (e.g. Hayes *et al.* 2013; Lay *et al.* 2013).

Geometric analyses of the combined polygons in all subduction zones can be broken into three groups: (1) subduction zones with no resolvable broad geometric barriers, (2) subduction zones with few, dispersed, resolvable broad geometric barriers and (3) subduction zones with frequent, resolvable broad geometric barriers. The group 1 models are: Cascadia, Izu-Bonin/Mariana, Kamchatka/Kuril/Japan, Makran, New Guinea and South America. These models generate a polygon that encompasses the entire seismogenic zone. The group 2 models are: Alaska/Aleutians, Caribbean, Central America, Kermadec/Tonga, Ryukyu/Nankai, Sulawesi and Sumatra/Java. These models usually exhibit large patches of potential rupture that are either in one block (e.g. Central America) or multiple large segments (e.g. Kermadec/Tonga). The final group of models either reveals a total lack of flat area large enough to host M 8 + ruptures (Cotabato, Manila, Vanuatu) or results in small disconnected patches of flat seismogenic zone capable of hosting M∼8 ruptures (e.g. Calabria, Himalaya, Philippines and Solomon Islands).

DISCUSSION

A variety of bathymetric features entering subduction zones have been proposed to act as barriers to earthquake ruptures. Rather than presenting an exhaustive list here, we refer readers to the review presented in Bilek & Lay (2018) and Philibosian & Meltzner (2020). These summaries illustrate the variety of features proposed to alter subduction zone topography and impede the propagation of megathrust rupture. The mechanical explanation for rupture arrest in these regions would presumably be analogous to the model proposed by Bletery *et al.* (2016) and discussed in greater detail in Bletery *et al.* (2017). Examples include the Juan Fernandez, Nazca and Carnegie Ridges in South America (e.g. Gutscher *et al.* 1999; Bilek 2010); the Tehuantepec Ridge in Mexico (e.g. Astiz & Kanamori 1984); a megathrust 'saddle' coinciding with the subduction of the 96°E fracture zone beneath Simeulue Island (e.g. Briggs *et al.* 2006), and the Wharton Fossil Ridge (Philibosian & Meltzner 2020), both offshore Sumatra; and the Gizo fracture zone in the Solomon Islands

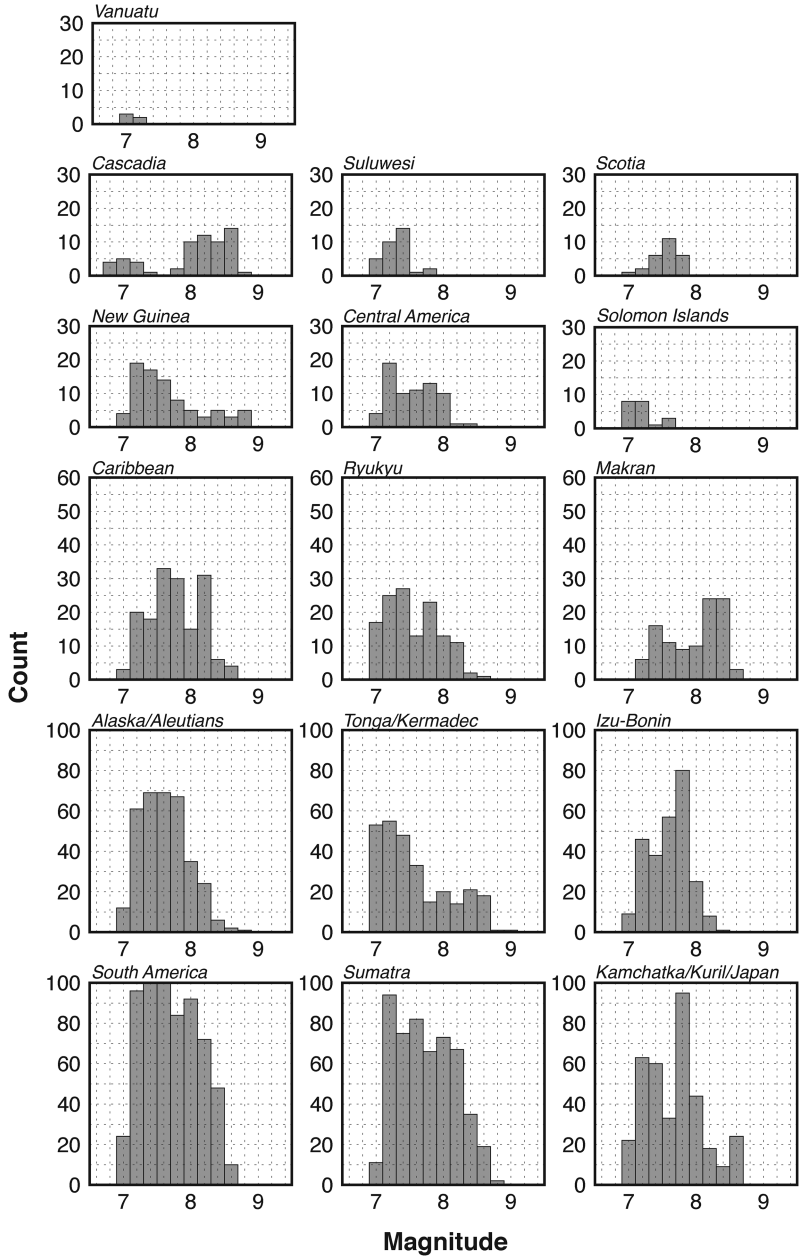

Figure 3. Magnitude distributions of large individual polygons identified in our joint Ks–Kt planarity search. For each subduction zone, we show the number and equivalent sizes of polygons large enough to host M 7 + earthquakes, based on seismogenic zone geometry characteristics.

(e.g. Furlong *et al.* 2009). These themes are also generally consistent with the idea that seafloor roughness plays a role in the size and extent of megathrust earthquakes, as examined extensively in van Rijsingen *et al.* (2018), where the authors demonstrate that large earthquakes, and in particular the location of asperities, correlate with the locations of smooth seafloor outboard of the trench.

In order to examine some of these subducting bathymetric features in more detail, we create cross sections of Ks and Kt along the 20 km slab depth contour. In Figs 7 and 8, we explore the expression of these features in our models of seismogenic zone planarity. We also analyze the along-strike density of individual polygons derived from the earlier part of our analysis (Figs 1 and 2), under the assumption that if barriers exert control on the megathrust, planarity should be affected and thus there should be fewer (or no) regions capable of hosting large earthquakes. We note that Slab2 has a resolution of $\sim 0.1^{\circ}$ in regions of highest data quality, meaning it would be difficult for our model to detect anomalies <10 km in width or length. Figs 7 and 8 show that the planarity of the seismogenic zones in South America and Sumatra do not clearly deviate enough from the statistical geometrical properties of the rupture areas of past great-sized earthquakes to make these features stand out as potential persistent barriers to rupture, though there does appear to be some correlation between the along-strike density of large polygons and Ks in particular (which is to be expected). Nevertheless, there does not appear to be a clear threshold in Ks or Kt that would mark these subducting bathymetric features as clear barriers to rupture.

There are several reasons why these proposed barriers may not be identified as such in our model. The first and simplest expla-

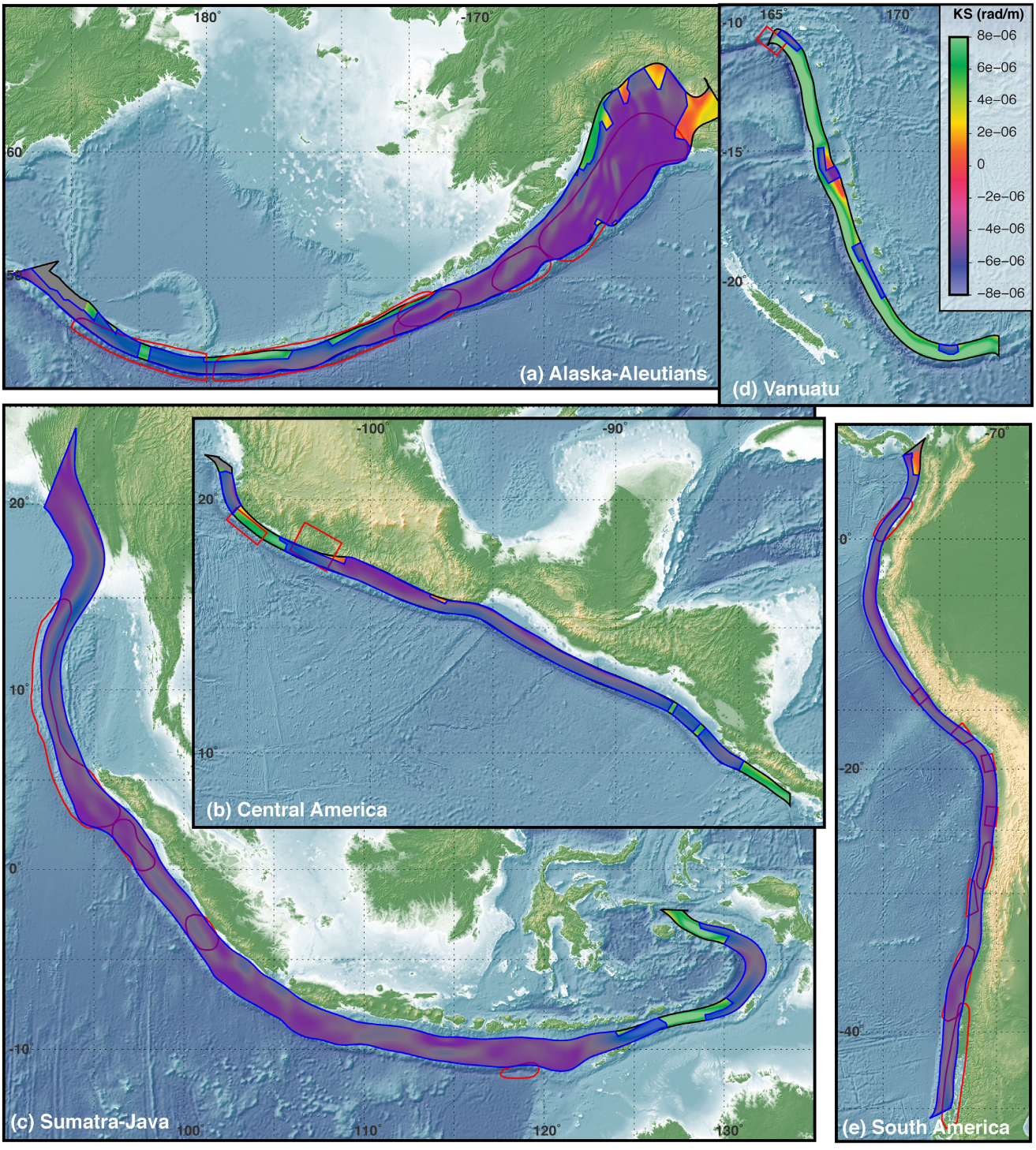

Figure 4. Combined polygons for (a) Alaska-Aleutians, (b) Central America, (c) Sumatra-Java, (d) Vanuatu and (e) South America, differentiating regions from our planarity searches that have overlapping polygons (blue shaded regions) with those without polygons (unshaded). Background colours for each slab are along-dip curvature, Ks. These polygons are used to calculate M_{flat} in Table 1. Fig. S1 shows the same regions without combined polygons overlain.

nation is that these regions do not exert a dominant control on a propagating rupture from the perspective of subduction zone geometry (i.e. if they are barriers, then some other property of the megathrust region or of the propagating rupture dominates rupture termination). As discussed earlier, several authors have proposed alternative models for rupture control, including trench sediment fill, buoyancy,and forearc structure. Bletery *et al.* (2017) attempt to quantify the Bletery *et al.* (2016) planarity model by examining the spatial variability in shear strength along the megathrust, which they model as a combination of slab geometry, stress state and convergence obliquity. Accounting for such other factors in our analysis may provide further insights into future great-sized earthquake potential. A second possibility is that barrier features such as these do not modify subduction zone topography enough to be

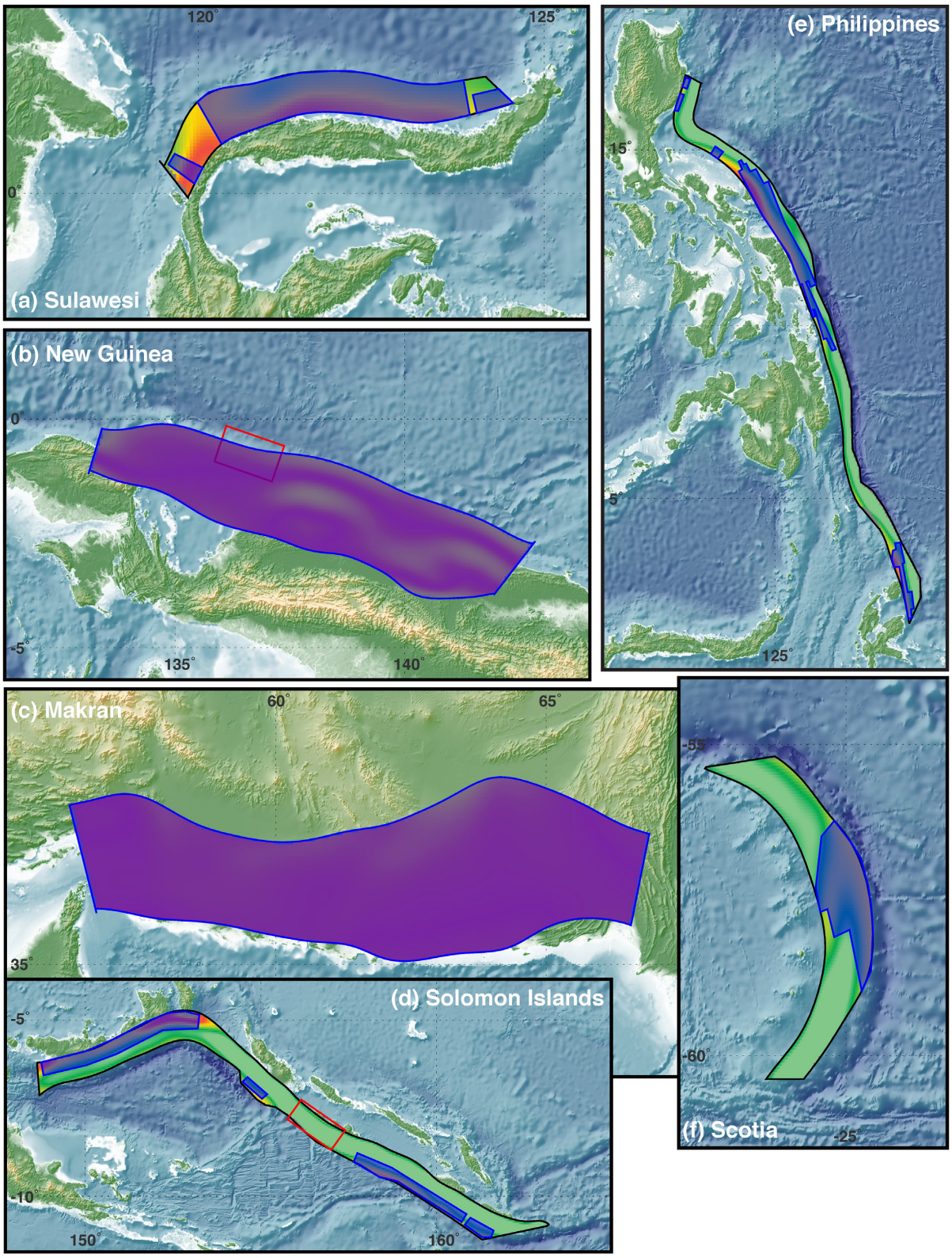

Figure 6. Combined polygons for (a) Sulawesi, (b) New Guinea, (c) Makran, (d) Solomon Islands, (e) Philippines and (f) Scotia, differentiating regions from our planar searches that have overlapping polygons (blue shaded regions) with those without polygons (unshaded). Background colours for each slab are along-dip curvature, KS. These polygons are used to calculate M_{flat} in Table 1. See also Fig. 4. Fig. S3 shows the same regions without combined polygons overlain.

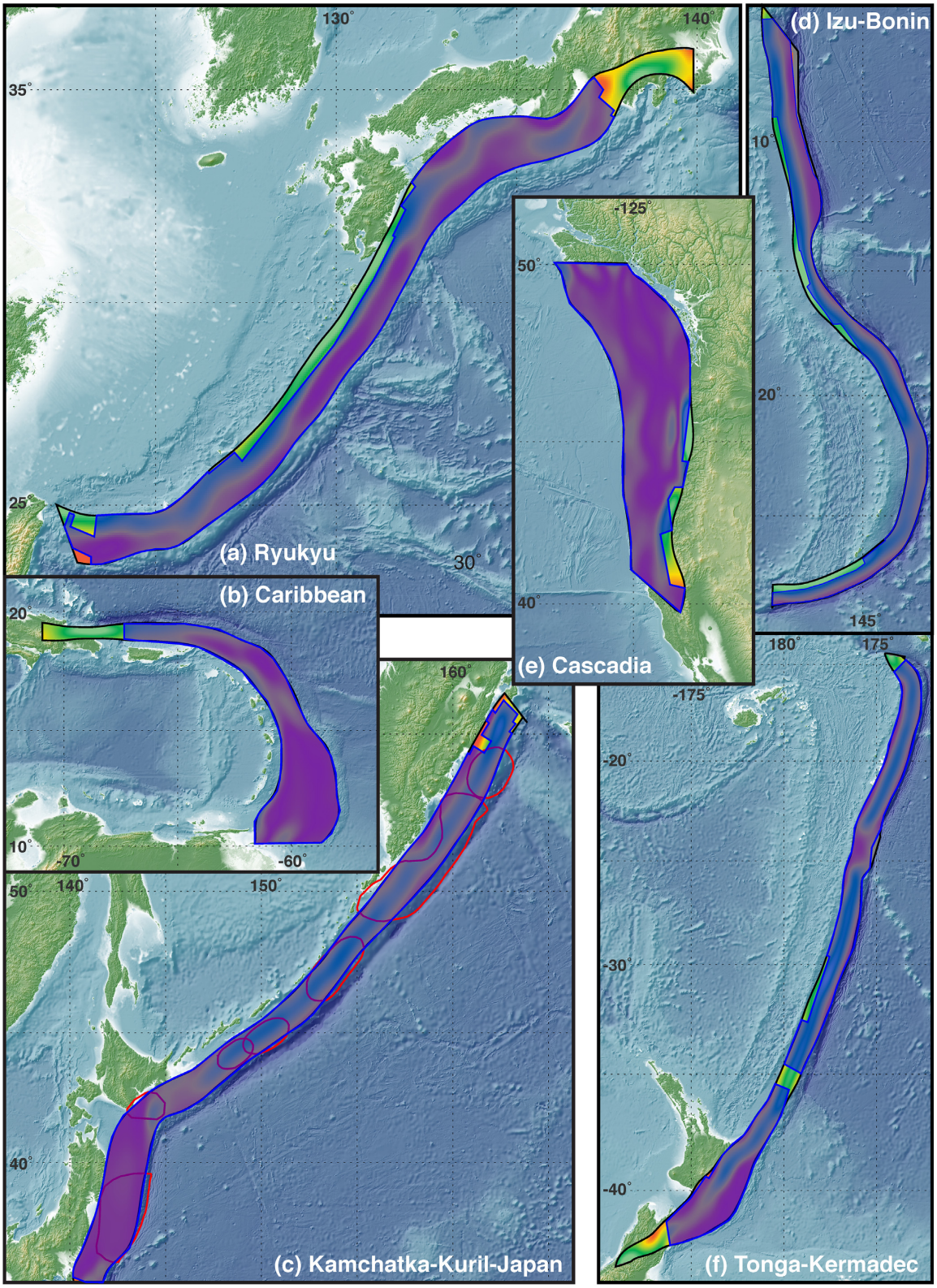

Figure 5. Combined polygons for (a) Ryukyu, (b) Caribbean, (c) Kamchatka-Kuril-Japan, (d) Izu-Bonin, (e) Cascadia and (f) Tonga-Kermadec, differentiating regions from our planar searches that have overlapping polygons (blue shaded regions) with those without polygons (unshaded). Background colours for each slab are along-dip curvature, Ks. These polygons are used to calculate M_{flat} in Table 1. See also Fig. 4. Fig. S2 shows the same regions without combined polygons overlain.

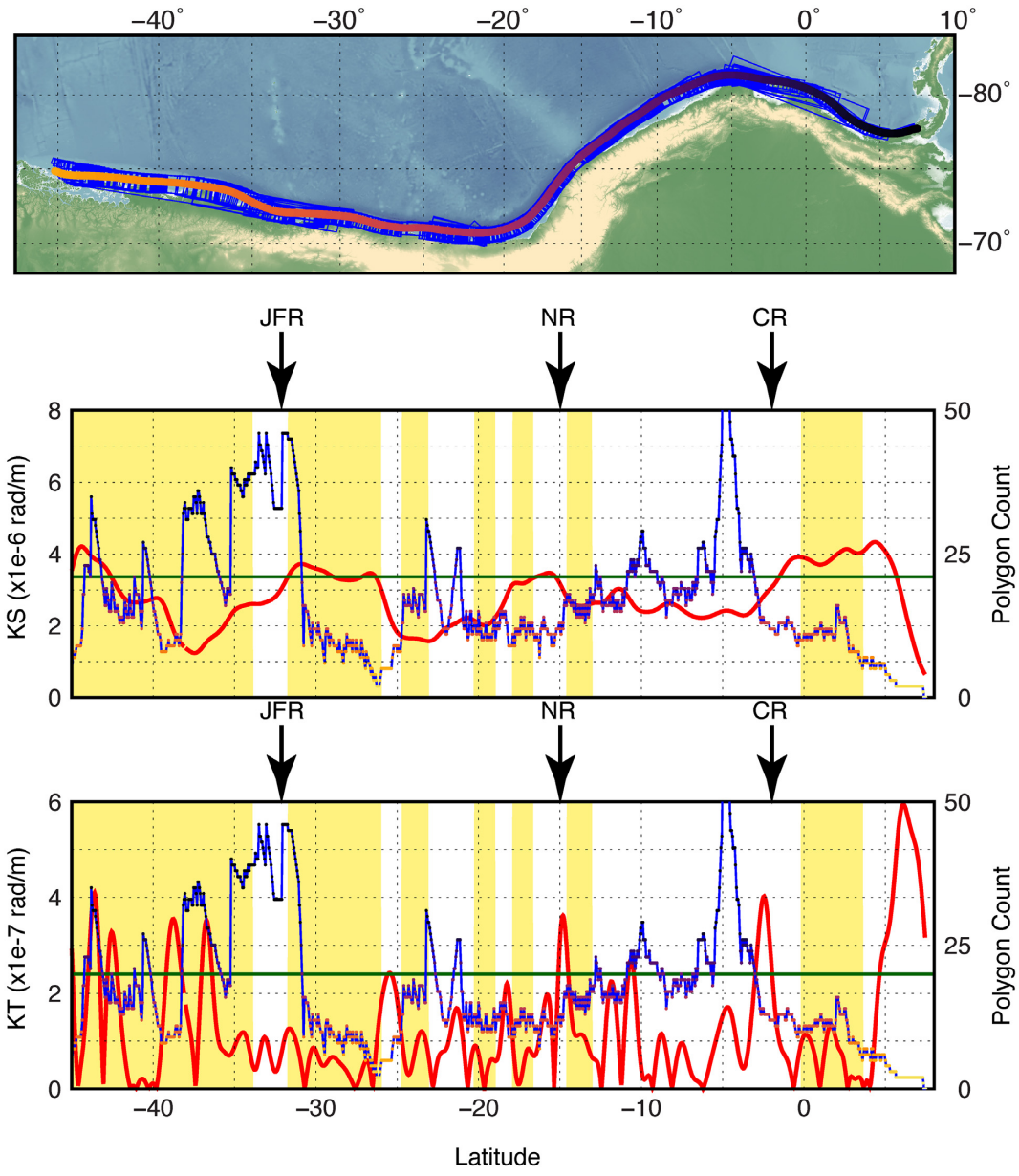

Figure 7. Along-strike cross section of along-dip (Ks, middle panel) and along-strike (Kt, bottom panel) planarity versus latitude along the 20 km depth contour for South America (red solid line in each panel). Superimposed on each panel is the along-strike density of large polygons identified in our planarity search (blue solid line). A map of the study region is shown in the top panel. The global target value for each of Ks and Kt is represented by the green horizontal line. The rupture areas of historical earthquakes are outlined in yellow and the major bathymetric features (potential barriers to earthquake rupture) are marked with an arrow at the location they enter the trench. JFR, Juan de Fuca Ridge; NR, Nazca Ridge; CR, Carnegie Ridge.

appropriately expressed in the Slab2 geometry model (i.e. they are too small or too short in wavelength). A third possibility is that barriers may not completely arrest rupture, but instead slow down rupture enough to cause the rupture to stop shortly after a rupture front encounters a barrier (e.g. Philibosian *et al.* 2020). This would mean that the geometric expression of barriers is included in the target planarity statistics of (at least some) historical ruptures, and thus searching for those properties elsewhere in subduction zones will make it difficult to identify other barrier-like features as being anomalous.

Whether or not these particular bathymetric features act as barriers within their respective seismogenic zones, our quantitative analysis of the Bletery *et al.* (2016) hypothesis reveals that there are significant differences in the planarity of megathrust zones globally. If we believe that the observation of historical great-sized earthquakes occurring along planar portions of megathrusts (Bletery *et al.* 2016) indicates a future likelihood for great-sized earthquakes to also occur in regions with similar geometrical characteristics, then these differences imply we can classify subduction zone megathrust hazard according to planarity statistics. These statistics are summarized

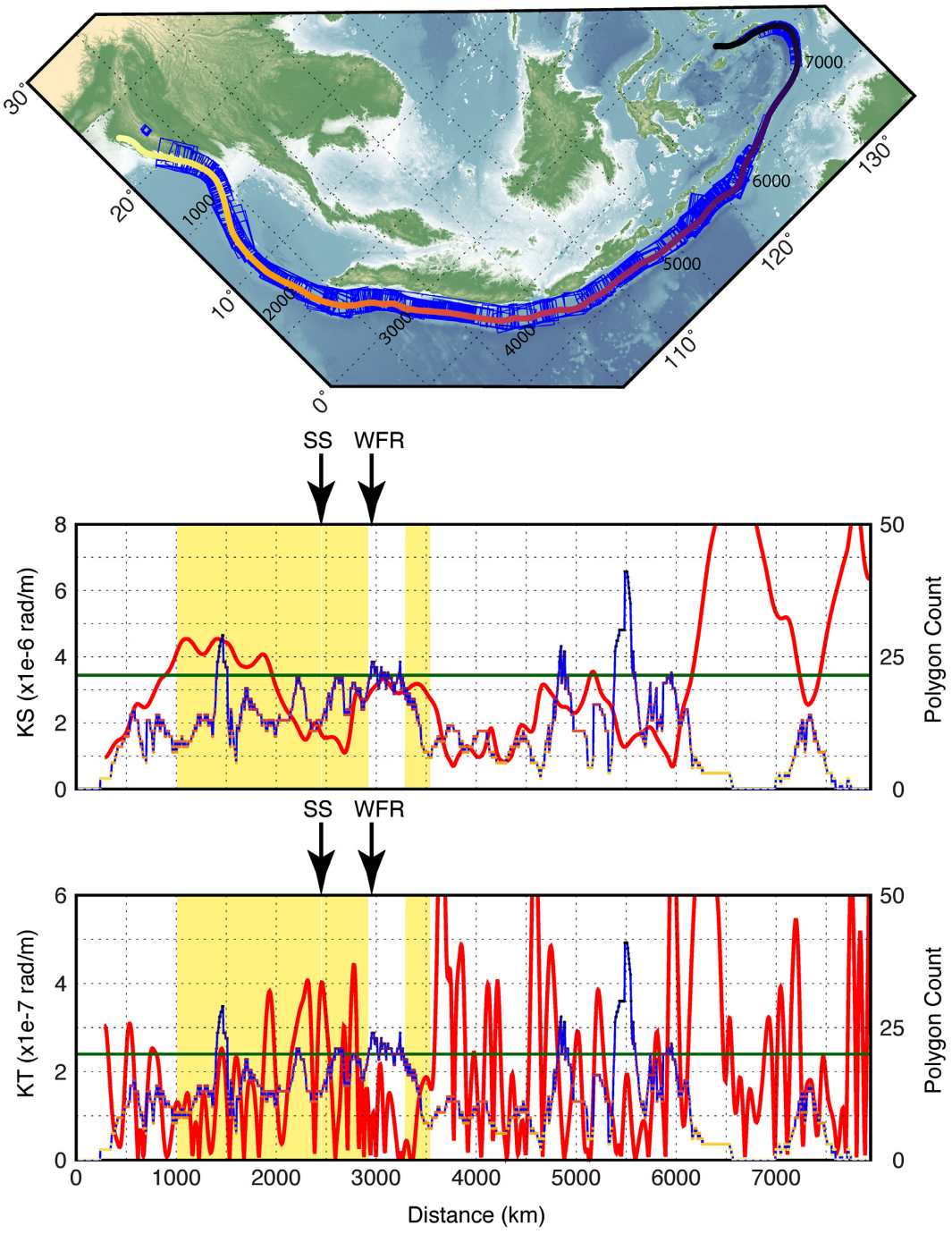

Figure 8. Along-strike cross-section of along-dip (Ks, middle panel) and along-strike (Kt, bottom panel) planarity versus distance along strike following the 20 km depth contour for Sumatra-Java (red solid line in each panel). Superimposed on each panel is the along-strike density of large polygons identified in our planarity search (blue solid line). A map of the study region is shown in the top panel. The global target value for each of Ks and Kt is represented by the green horizontal line. The rupture areas of historical earthquakes are outlined in yellow and the major bathymetric features (potential barriers to earthquake rupture) are marked with an arrow at the location they enter the trench. SS, Simelue Saddle (subduction of the 96°E fracture zone); WFR, Wharton Fossil Ridge.

in Figs 1–3. Fig. 1 shows all of our modelled subduction zones and their corresponding mean Ks and Kt. The more planar subduction zones (the ones on the left of Fig. 1) are in general more likely to host great-sized megathrust earthquakes than the subduction zones that exhibit higher curvature (on the right of Fig. 1). The most planar subduction zones identified in Fig. 1 also host both the greatest number and the largest polygons in our analysis of planarity extent, from which one may infer they are capable of hosting the largest sized earthquakes (Figs 2 and 3) and can do so more frequently (depending on strain accumulation rates).

This observation is, however, not without exception; some subduction zones with average geometric characteristics more variable than our target planarity threshold (e.g. Vanuatu, Solomon Islands) have hosted a historical M 8 + event, while others (e.g. Makran or New Guinea) are extremely planar, but the maximum magnitude earthquake may not have occurred in our historical period

of observation (since 1900). Magnitude distributions of individual (Figs 2 and 3) and combined polygons (Fig. 4, M_{flat}) for all seismogenic zones are presented in Table 1. For several regions (Alaska-Aleutians, Kermadec, Kamchatka-Kuril-Japan and Sumatra-Java), we calculate M_{flat} of 9.5+, and interpret this to mean these seismogenic zones are more likely to be capable of hosting mega-sized events. Four of the five subduction zones with $M_{flat} = 9.5 +$ have hosted historical M 9 + earthquakes; the only exception is Tonga-Kermadec. For other seismogenic zones (Manila, Philippines, Scotia, Solomon Islands, Sulawesi and Vanuatu), we infer $M_{flat} <\sim 8.0$, and believe it would be difficult for these subduction zones to host mega earthquakes. In some instances (e.g. Manila, Vanuatu), our search does not identify an area that can accommodate even a M8.0 earthquake based on our curvature analysis and scaling relations. We interpret this to mean that these seismogenic zones are less likely to host a great-sized earthquake. A final group of subduction zones (e.g. Central America, Caribbean, Izu-Bonin, Makran, New Guinea, Ryukyu) have much larger M_{flat} values than their historical M_{max}, which is likely to indicate that either we have not yet experienced the largest earthquake these regions will host, or that other factors play a more dominant role in rupture control in such locations. Elsewhere, the M_{flat} calculated from the various scaling relations tends to be consistent with the maximum historical magnitude in subduction zones whose Slab2 geometry models are well constrained (Hayes *et al.* 2018).

CONCLUSIONS

Our analysis has illuminated details about subduction zone geometric constraints on megathrust earthquakes. We show that it is possible, based on slab curvature alone, for many subduction zones to host great-sized earthquakes. In several subduction zones, this may occur within single slip patches; in other regions, while great-sized events are still possible, they may require multiple patches rupturing simultaneously. Consistent with the results of Bletery *et al.* (2016), we also find that many historical megathrust earthquakes are associated with broadly planar areas of subduction zones. Furthermore, all regions with documented M 9 + earthquakes historically are identified as being capable of hosting similar sized events in the future, despite the exclusion of those historical ruptures from our analysis. Conversely, if geometry plays a dominant control on rupture propagation, our analysis indicates it may be very difficult for some subduction zones to host great-sized earthquakes (e.g. Manila, Philippines and Vanuatu). Finally, our analysis shows that documented barriers to historical ruptures are not readily identifiable in along-strike and along-dip curvature, implying that they either are too localized to be distinguishable in Slab2 models, or that their influence on rupture propagation is not exerted via geometrical effects alone.

ACKNOWLEDGEMENTS

We thank the Editor Margarita Segou, an Associate Editor, reviewers Quentin Bletery, Nadav Wetzler, Belle Philibosian, Kirstie Haynie and an anonymous reviewer for their comments, which helped improve upon earlier versions of this manuscript. Any use of trade, product or firm names is for descriptive purposes only and does not imply endorsement by the U.S. Government. Global data sets used in this study are from the Advanced National Seismic System Comprehensive Catalogue (http://earthquake.usgs.gov/earthquakes/search/, USGS 2017), the EHB global relocated earthquake catalogue (Engdahl et al., 1998) and the Global CMT catalogue (Ekstrom et al., 2012). Figures were made with the Generic Mapping Tools software package (Wessel and Smith, 1991G38). Slab2 is openly available via ScienceBase (https://doi.org/10.5066/F7PV6JNV, doi:10.5066/F7PV6JNV). The Slab2 code base is available via GitHub (https://github.com/usgs/slab2).

REFERENCES

Allen, T.I. & Hayes, G.P., 2017. Alternative rupture scaling relationships for subduction interface and other offshore environments, *Bull. seism. Soc. Am.,* **107**(3), 1240–1253.

Astiz, L. & Kanamori, H., 1984. An earthquake doublet in Ometepec, Guerrero, Mexico, *Phys. Earth planet. Inter.,* **34**(1-2), 24–45.

Bassett, D., Sandwell, D.T., Fialko, Y. & Watts, A.B., 2016. Upper-plate controls on co-seismic slip in the 2011 magnitude 9.0 Tohoku-oki earthquake, *Nature,* **531**(7592), 92.

Bilek, S.L., 2010. Invited review paper: seismicity along the South American subduction zone: review of large earthquakes, tsunamis, and subduction zone complexity, *Tectonophysics,* **495**(1–2), 2:14.

Bilek, S.L. & Lay, T., 2018. Subduction zone megathrust earthquakes, *Geosphere,* **14**(4), 1468–1500.

Bletery, Q., Thomas, A.M., Rempel, A.W. & Hardebeck, J.L., 2017. Imaging shear strength along subduction faults, *Geophys. Res. Lett.,* **44,** 11 329–11 339.

Bletery, Q., Thomas, A.M., Rempel, A.W., Karlstrom, L., Sladen, A. & De Barros, L., 2016. Mega-earthquakes rupture flat megathrusts, *Science,* **354**(6315), 1027–1031.

Briggs, R.W., Sieh, K., Meltzner, A.J., Natawidjaja, D., Galetzka, J., Suwargadi, B., Hsu, Y-J., Simons, M., Hananto, N., Suprihanto, I., Prayudi, D., Avouac, J.-P., Prawirodirdjo, L. & Bock, Y., 2006. Deformation and Slip Along the Sunda Megathrust in the Great 2005 Nias-Simeulue Earthquake, *Science,* **311**(5769):1897–1901.

Davies, J., Sykes, L., House, L. & Jacob, K., 1981. Shumagin seismic gap, Alaska Peninsula: history of great earthquakes, tectonic setting, and evidence for high seismic potential, *J. geophys. Res.,* **86**(B5), 3821–3855.

Ekström, G., Nettles, M. & Dziewoński, A.M., 2012. The global CMT project 2004–2010: centroid moment tensors for 13,017 earthquakes, *Phys. Earth planet. Inter.,* **200–201,** 1–9.

Engdahl, E.R., Van Der Hilst, R.D. & Buland, R.P., 1998. Global teleseismic earthquake relocation with improved travel times and procedures for depth determination, *Bull. seism. Soc. Am.,* **88,** 722–743.

Furlong, K.P., Lay, T. & Ammon, C.J., 2009. A great earthquake rupture across a rapidly evolving three-plate boundary, *Science,* **324**(5924), 226–229.

Goda, K., Yasuda, T., Mori, N. & Maruyama, T., 2016. New scaling relationships of earthquake source parameters for stochastic tsunami simulation, *Coastal Eng. J.,* **58**(3), doi:10.1142/S0578563416500108.

Graham, S, DeMets, C, Cabral-Cano, E, Kostoglodov, V, Rousset, B, Walpersdorf, A, Cotte, N, Lasserre, C, McCaffrey, R & Salazar-Tlaczani, L, 2016. Slow slip history for the Mexico subduction zone: 2005 through 2011, *Pure and applied Geophysics,* **173,** 3445–3465.

Gutscher, M.A., Malavieille, J., Lallemand, S. & Collot, J.Y., 1999. Tectonic segmentation of the North Andean margin: impact of the Carnegie Ridge collision, *Earth Planet. Sci. Lett.,* **168,** 255–270.

Hayes, G.P., Furlong, K.P., Benz, H.M. & Herman, M.W., 2013. Triggered aseismic slip adjacent to the 6 February 2013 Mw 8.0 Santa Cruz Islands megathrust earthquake, *Earth and Planetary Science Letters,* **388,** 265–272.

Hayes, G.P., Moore, G.L., Portner, D.E., Hearne, M., Flamme, H., Furtney, M. & Smoczyk, G.M., 2018. Slab2, a comprehensive subduction zone geometry model, *Science,* **362**(6410), 58–61.

Hayes, G.P., Wald, D.J. & Johnson, R.L., 2012. Slab1.0: a three dimensional model of global subduction zone geometries, *J. geophys. Res.,* **117,** B01302, doi:10.1029/2011JB008524.

Heuret, A., Conrad, C.P., Funiciello, F., Lallemand, S. & Sandri, L., 2012. Relation between subduction megathrust earthquakes, trench sediment

thickness and upper plate strain, *Geophys. Res. Lett.,* **39,** L05304, doi:10.1029/2011GL050712.
Hough, S.E., 2013. Missing great earthquakes, *J. geophys. Res.,* **118,** 1098–1108.
Lay, T., Kanamori, H., Ammon, C.J., Koper, K.D., Hutko, A.R., Ye, L., Yue, H. & Rushing, T.M., 2012. Depth-varying rupture properties of subduction zone megathrust faults, *J. geophys. Res.,* **117,** B04311, doi:10.1029/2011JB009133.
Lay, T., Ye, L., Kanamori, H., Yamazaki, Y., Cheung, K.F. & Ammon, C.J., 2013. The February 6, 2013 Mw 8.0 Santa Cruz Islands earthquake and tsunami, *Tectonophysics,* **608,** 1109–1121.
Leonard, M., 2010. Earthquake fault scaling: self-consistent relating of rupture length, width, average displacement, and moment release, *Bull. seism. Soc. Am.,* **100**(5A), 1971–1988.
Mai, M.P. & Beroza, G.C., 2000. Source scaling properties from finite-fault-rupture models, *Bull. seism. Soc. Am.,* **90**(3), 604–615.
Muratoni, S., Satake, K. & Fujii, Y., 2013. Scaling relations of seismic moment, rupture area, average slip, and asperity size for *M*∼9 subduction zone earthquakes, *Geophys. Res. Lett.,* **40,** 5070–5074.
Nishikawa, T. & Ide, S., 2014. Earthquake size distribution in subduction zones linked to slab buoyancy, *Nat. Geosci.,* **7,** 904–908.
Philibosian, B. & Meltzner, A.J., 2020. Segmentation and supercycles: A catalog of earthquake rupture patterns from the Sumatran Sunda Megathrust and other well-studied faults worldwide, *Quaternary Science Reviews,* in press.
Ruff, L. & Kanamori, H., 1980. Seismicity and the subduction process, *Phys. Earth planet. Inter.,* **23,** 240–252.
Satake, K., Shimazaki, K., Tsuji, Y. & Ueda, K., 1996. Time and size of a giant earthquake in Cascadia inferred from Japanese tsunami records of January 1700, *Nature,* **379,** 246–249.
Skarlatoudis, A.A., Somerville, P.G. & Thio, H.K., 2016. Source scaling relations of interface subduction earthquakes for strong ground motion and tsunami simulation, *Bull. seism. Soc. Am.,* **106**(4), 1652–1662.
Song, T.-R.A. & Simons, M., 2003. Large trench-parallel gravity variations predict seismogenic behavior in subduction zones, *Science,* **301,** 630–633.
Suárez, G. & Albini, P., 2009. Evidence for great tsunamigenic earthquakes (*M* 8.6) along the Mexican subduction zone, *Bull. seism. Soc. Am.,* **99,** 892–896.
,U.S. Geological Survey, Earthquake Hazards Program, 2017. Advanced National Seismic System (ANSS) Comprehensive Catalog of Earthquake Events and Products: Various, *https://doi.org/10.5066/F7MS3QZH,* .
Uyeda, S. & Kanamori, H., 1979. Back-arc opening and the mode of subduction, *J. geophys. Res.,* **84,** 1049–1061.
van Rijsingen, E., Lallemand, S., Peyret , M., Arcay , D., Heuret , A., Funiciello, F. & Corbi, F., 2018. How Subduction Interface Roughness Influences the Occurrence of Large Interplate Earthquakes, *Geochemistry, Geophysics, Geosystems,* **19,** 2342–2370.
Wessel, P. & Smith, W.H.F., 1991. Free software helps map and display data, *EOS, Trans. Am. Geophys. Un.,* **72,** 441–446.
Ye, L., Lay, T., Kanamori, H. & Rivera, L., 2016. Rupture characteristics of major and great (*Mw* ≥ 7.0) megathrust earthquakes from 1990 to 2015: 1. Source parameter scaling relationships, *J. geophys. Res.,* **121,** 826–844.U

SUPPORTING INFORMATION

Supplementary data are available at *GJI* online.

Figure S1. Along-dip planarity (Ks, rad m^{-1}) for (a) Alaska-Aleutians, (b) Central America, (c) Sumatra—Java, (d) Vanuatu and (e) South America calculated from the Slab2 subduction zone geometry model.
Figure S2. Along-dip planarity (Ks, rad m^{-1}) for (a) Ryukyu, (b) Caribbean, (c) Kamchatka—Kuril—Japan, (d) Izu—Bonin, (e) Cascadia and (f) Tonga—Kermadec calculated from the Slab2 subduction zone geometry model.
Figure S3. Along-dip planarity (Ks, rad m^{-1}) for (a) Sulawesi, (b) New Guinea, (c) Makran, (d) Solomon Islands, (e) Philippines and (f) Scotia calculated from the Slab2 subduction zone geometry model.
Figure S4. Along-strike planarity (Kt, rad m^{-1}) for (a) Alaska-Aleutians, (b) Central America, (c) Sumatra—Java, (d) Vanuatu and (e) South America calculated from the Slab2 subduction zone geometry model.
Figure S5. Along-strike planarity (Kt, rad m^{-1}) for (a) Ryukyu, (b) Caribbean, (c) Kamchatka—Kuril—Japan, (d) Izu—Bonin, (e) Cascadia and (f) Tonga—Kermadec calculated from the Slab2 subduction zone geometry model.
Figure S6. Along-strike planarity (Kt, rad m^{-1}) for (a) Sulawesi, (b) New Guinea, (c) Makran, (d) Solomon Islands, (e) Philippines and (f) Scotia calculated from the Slab2 subduction zone geometry model.
Figure S7. Comparison of along-dip planarity (Ks) vs the maximum magnitude observed for each subduction zone. Top left-hand panel**:** a recreation of Fig. 2 from Bletery *et al.* (2016) using the Slab1.0 subduction zone model. Top right-hand panel: we substitute new maximum magnitudes for some subduction zones (See Table S1) and improve the linear correlation using Slab1.0. Bottom panel**:** we further update this correlation using Slab2 to calculate Ks. The correlation is slightly reduced, but still close to the original correlation value of 0.8.
Figure S8. Sensitivity tests describing how varying the target along-dip planarity, Ks_{tar}, in South America affects areas our analysis. Compared to Fig. 4(e), incrementally reducing Ks_{tar} leads to fewer historical rupture areas being identified as being sufficiently planar for future large earthquake rupture.
Figure S9. Linear fits between along dip (Ks) and along strike (Kt) planarity (a) Contains subduction zones from Slab2 with N-data <40, where *N* is the number of shallow thrust-type interface earthquakes in a given subduction zone. These subduction zones tend to result in anomalously high Kt values. Correlation coefficient of $r = \sim 0.62$ (b) Removal of low N-data models from our analyses results in a better correlation coefficient of $r = \sim 0.70$.
Table S1. A list of all global *M* 8 + post-1900 earthquakes, including references and descriptions of whether or not they have been included in our analysis.

Please note: Oxford University Press is not responsible for the content or functionality of any supporting materials supplied by the authors. Any queries (other than missing material) should be directed to the corresponding author for the paper.